Development of Adaptive Rubber Bearings

C. S. Tsai[1], H. C. Su[2], W. C. Huang[3], T. C. Chiang[4]

[1,3]*Department of Civil Engineering, Feng Chia University, Taichung, Taiwan*

[2]*Department of Water Resources Engineering and Conservation, Feng Chia University, Taichung, Taiwan*

[4]*Earthquake Proof Systems, Inc., Taichung, Taiwan*

ABSTRACT

A new seismic isolator made of rubber material is proposed in this study. This seismic isolator is called the adaptive rubber bearing (ARB) because of its adaptive characteristic. The lead material which is usually found in lead rubber bearing (LRB) results in heavy environmental burden and lower yield strength and damping due to rising temperature during earthquakes, causing larger displacements than we would expect. The designed mechanisms in the proposed seismic isolator make this device relatively easily manufactured and also provide extremely high damping to the bearing, which is highly desired by engineers in practice. The proposed rubber bearing that uses lead-free materials is completely passive device yet possesses adaptive stiffness and adaptive high damping. The change in stiffness and damping is predicable and can be calculated at specifiable and controllable displacement amplitudes. The major advantage of the adaptive characteristic of a seismic isolator is that a given system can be optimized separately for multiple performance objects at multiple levels of earthquakes. In this paper, theoretical formulations have been derived to explain the mechanical mechanisms of the proposed device. Experimental results are also provided to validate the advanced concept of the proposed isolator.

Keywords: *Seismic isolation systems; High damping; Adaptive device; Passive control; Earthquake engineering; Earthquake proof systems*

1 INTRODUCTION

Base isolation technology that minimizes the seismic responses of a structure by introducing a flexible connection between the structure and the ground to move away the natural period of a structure from the predominant period of the ground motion, has been recognized worldwide as a promising technique to protect existing and new structures from earthquake damage. This has been verified through extensive experimental and numerical studies as well as field measurements taken during earthquakes. Among the techniques [1-5] achieving a flexible connection and having gained acceptance, two types of popular seismic isolation systems have been certified to efficiently mitigate the seismic responses of structures. These are the elastomeric bearing-based [6-8] and sliding-based systems [9-19]. The American L. Sterne [20] in 1869, stated concerning his invention:

[1] Distinguished Professor, cstsai@mail.fcu.edu.tw

[2] Associate Professor, hcsu@fcu.edu.tw

[3] Master Student, outside369842@yahoo.com.tw

[4] Technical Manager, rickchiang19771011@gmail.com

* Corresponding author: C. S. Tsai

"My invention consists of a novel construction of spring, more particularly applicable to or as buffers, bearing and drawing springs for railway purposes, which is of the character of a pneumatic rubber spring, and is made or built up of soft India-rubber rings, and circular or other suitable shaped metal-plates, the rubber rings being chemically united to the plates during the process of vulcanization, and being alternately arranged in relation to said plates...". This device was proposed as a bearing for railway purposes, not intended as a means for seismic isolation. However, it already represented an embryonic form of chemically uniting alternately arranged plates and rubber layers during the process of vulcanization and curing. It could function as a modern seismic isolator. Robinson [8] of New Zealand in 1978 increased the damping ratio of the device by inserting a lead core into the center of the system proposed by Sterne in 1869. Robinson's lead rubber bearing (LRB) could be, if manufactured up-to-date, the most popular rubber bearing in engineering applications in the world. However, the lead material used in a LRB results in heavy environmental burden as well as lower yield strength and damping resulting from rising temperatures during earthquakes, which leads to larger displacements than we would expect.

In this study, a new type of seismic isolator composed of rubber materials and called the adaptive rubber bearing (ARB) is proposed to tackle the aforementioned problems encountered by LRBs. This isolator utilizes nature-friendly materials and is lead-free. The proposed seismic isolator is completely passive, yet possesses adaptive characteristics of stiffness and damping. Its change in stiffness and damping is predictable and can be calculated at controllable displacement amplitudes. In addition to achieving adaptive behaviour, the proposed rubber bearing possesses an extremely high damping ratio of approximately 60% at small displacements, which is desired by engineers in practice. In this study, mathematical formulations are derived to explain the mechanisms of the proposed bearing. In addition, experimental results are provided to verify the concepts of the proposed device. The proposed isolator has the following advantages while compared to the LRB: (1) utilizes environmentally friendly materials, (2) has fewer temperature rising problems, (3) distributes uniform force without stress concentration at specific areas of the energy absorption core, (4) has much higher damping, (5) possesses adaptive characteristics, (6) is easier to manufacture, (7) is lighter, (8) allows for the deformation of rubber layers to be optimized individually for multiple performance objects at multiple levels of earthquakes, and (9) has independently adjustable vertical stiffness obtained from combinations of various materials of sliding plates without coupling with the horizontal stiffness provided by rubber.

2 CONCEPTS OF PROPOSED ADAPTIVE RUBBER BEARINGS

An LRB uses the heavy metal of lead to absorb vibration energy by yielding the lead material that induces a major burden on the environment. The yield point of the lead material is a function of ambient temperature and rising temperature derived from absorbed seismic energy. To solve the aforementioned problems encountered by the LRB, a series of innovative seismic isolators have been proposed Tsai et al. [21] in 2016. The major concepts behind the proposed isolator is described as follows. As Figs. 1 and 2 show, the seismic isolator consists of alternate rubber layers and shim plates like traditional rubber bearings. However, the major contribution of the proposed device is the new sliding core, which includes multiple sliding plates at each layer to have multiple sliding surfaces that are located between and confined by two adjacent shim plates. This helps in leveling the arrangements of shim plates and rubber materials during manufacturing processes. These sliding plates also distribute the displacement of a single layer into multiple sliding interfaces and smooth the sliding motion during earthquakes. This yields a smaller displacement and reduces the amount of heat derived from the friction of the sliding motion on each sliding plate of a single layer. The friction coefficient can be different from one sliding interface or rubber layer to another to control the time required to initiate the sliding motion of a sliding plate in a layer.

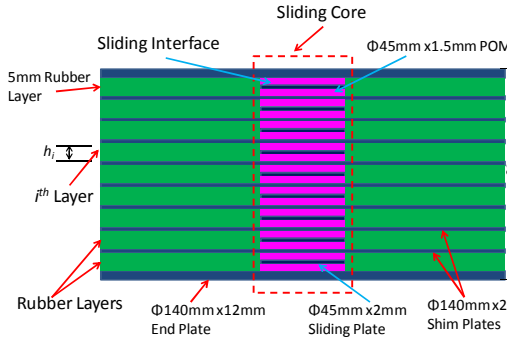

Figure 1 - Cross sectional view of adaptive rubber bearing (3 sliding plates in each layer)

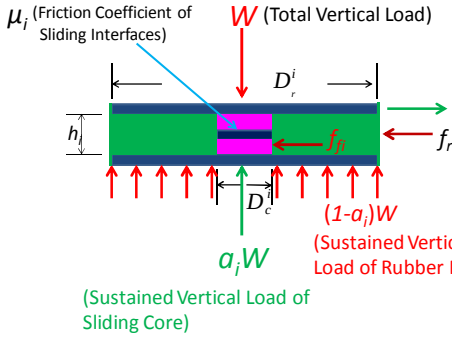

Figure 2 - Forces in a typical single layer of ARB isolator

The multiple sliding plates are confined between two adjacent shim plates to smooth the sliding motion and achieve adaptive functions on the basis of friction coefficients of these sliding interfaces. The sliding surfaces of each layer of the sliding core provide the device with extremely high damping in addition to adaptive functions. This is accomplished by controlling the deformation contribution of the rubber layer based on the predefined frictional force on each sliding surface. No deformation or sliding motion will occur at a specific rubber layer if the horizontal force of the device is smaller than the frictional force of a sliding interface in that particular layer. The layer will not induce damping in the system. In addition, the stiffness of the particular layer will be infinite. Any one of the sliding interfaces in a specific layer will be activated and begin sliding to produce damping if the horizontal force is greater than the frictional force of this particular sliding interface of this layer. Simultaneously, the rubber within the activated sliding plate in this activated layer will begin to deform, which will contribute to damping and stiffness. The mechanical behavior of the entire bearing is based on the series connections of activated layers. The major parameters for controlling the adaptive characteristics of the entire system are the friction coefficient and sustained vertical load at each sliding interface. In general, the adaptive functions can be achieved by adjusting the friction coefficients, sizes of sliding plates, and the thickness and material properties of rubber layers. These in turn adjust the vertical stiffness, sustained vertical loads, and frictional forces on the sliding plates and sliding interfaces. Many possible combinations of the aforementioned parameters can be adjusted to achieve multiple performance targets at multiple levels of earthquakes.

3 DERIVATION OF EFFECTIVE STIFFNESS AND EQUIVALENT DAMPING OF ARB

This section derives the mathematical formulations to illustrate the major concepts of the proposed isolator. Fig. 2 denotes the forces in a typical single layer. The rubber and multiple sliding plates of the sliding core in a single layer are connected in parallel. Therefore, the total horizontal force, F_i, in a single layer is the sum of the shear force of rubber and the frictional force of the sliding plates; that is

$$F_i = f_{ri} + f_{fi} = (k_{eff}^{ri} + k_{eff}^{fi})u_i = k_{eff}^{i} u_i \tag{1}$$

where f_{ri} is the shear force of the i^{th} layer of the rubber material; f_{fi} represents the frictional force of the sliding interface; u_i denotes the relative displacement between the top and bottom of the i^{th} layer; k_{eff}^{ri} is the effective stiffness of rubber material in the i^{th} layer, as shown in Fig. 3; and k_{eff}^{fi} indicates the effective stiffness of the sliding plate in the i^{th} layer, as shown in Fig. 4. In addition, k_{eff}^{i} represents the total effective stiffness of the i^{th} layer, which means that $k_{eff}^{i} = k_{eff}^{ri} + k_{eff}^{fi}$ and

$k_{eff}^{ri} = G_r^i A_r^i / h_i$ [6], where G_r^i, h_i, and A_r^i are the shear modulus, thickness, and cross-sectional area of rubber in the i^{th} layer, respectively.

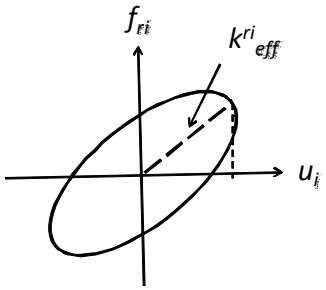

Figure 3 - Hysteretic loop of a single layer of rubber material

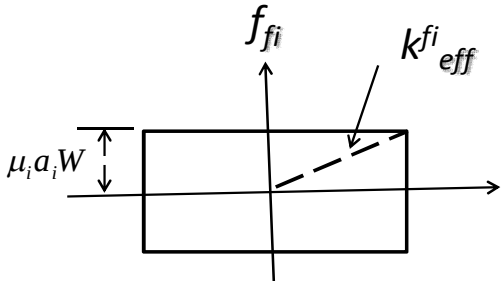

Figure 4 - Hysteretic loop of sliding core in a single layer

The total enclosed area, A_i, of the force-displacement loop of the i^{th} layer is the sum of the rubber, A_{ri}, and the sliding plates, A_{fi}. It is obtained as:

$$A_i = A_{ri} + A_{fi} \tag{2}$$

As shown in Fig. 3, the enclosed area of the force-displacement loop of the sole rubber of the i^{th} layer can be expressed as:

$$A_{ri} = 2\pi k_{eff}^{ri} u_i^2 \xi_{ri} \tag{3}$$

where ξ_{ri} denotes the equivalent damping ratio of the sole rubber in the i^{th} layer.

As seen in Fig. 4, the enclosed area of the force-displacement loop of sole sliding plates of the i^{th} layer is given by:

$$A_{fi} = 4u_i f_{fi} = 4(\mu_i a_i W)u_i \tag{4}$$

where a_i denotes a percentage of the total vertical load sustained by the sliding plates (this is derived later); and W is the total vertical load sustained by the bearing resulting from the dead and seismic loads.

The effective stiffness of sliding plates of the i^{th} layer, k_{eff}^{fi}, is obtained as:

$$k_{eff}^{fi} = \frac{f_{fi}}{u_i} = \frac{\mu_i a_i W}{u_i} \tag{5}$$

The total effective stiffness of the i^{th} layer, which includes the rubber and sliding plates, is given by:

$$k_{eff}^{i} = k_{eff}^{ri} + \frac{\mu_i a_i W}{u_i} \tag{6}$$

The total area enclosed by the hysteretic loop of the device, A, is the sum of the areas enclosed by the active rubber layers and the friction forces of the activated sliding interfaces in the sliding core. Assuming that the n^{th} layer is not activated, then the total area is obtained by excluding the effects of the n^{th} layer as:

$$A = \sum_{\substack{i=1 \\ i \neq n}}^{N} \left(A_{ri} + A_{fi}\right) = \sum_{\substack{i=1 \\ i \neq n}}^{N} (2\pi k_{eff}^{ri} u_i^2 \xi_{ri} + 4a_i W \mu_i u_i) \tag{7}$$

where N denotes the total number of layers in the device.

The total horizontal force of the i^{th} layer can be obtained as:

$$F_i = (k_{eff}^{ri} + k_{eff}^{fi})u_i = k_{eff}^{ri} u_i + a_i W \mu_i \tag{8}$$

Rearranging Eq. (8) yields a relative displacement between the top and bottom of the i^{th} layer; that is

$$u_i = \frac{F_i - a_i W \mu_i}{k_{eff}^{ri}} \tag{9}$$

If the horizontal force sustained by the sliding plates is smaller than the frictional force at the n^{th} layer that is $a_n W \mu_n$, the total displacement u of the isolator is the sum of the displacements of all layers except for the n^{th} layer and given by:

$$u = \sum_{\substack{i=1 \\ i \neq n}}^{N} u_i = \sum_{\substack{i=1 \\ i \neq n}}^{N} \frac{F_i - a_i W \mu_i}{k_{eff}^{ri}} = F \sum_{\substack{i=1 \\ i \neq n}}^{N} \frac{1}{k_{eff}^{ri}} - \sum_{\substack{i=1 \\ i \neq n}}^{N} \frac{a_i W \mu_i}{k_{eff}^{ri}} \tag{10}$$

The total horizontal force of the entire isolator can be obtained with the aid of Eq. (10) as:

$$F = \frac{1}{\sum_{\substack{i=1 \\ i \neq n}}^{N} \frac{1}{k_{eff}^{ri}}} u + \frac{1}{\sum_{\substack{i=1 \\ i \neq n}}^{N} \frac{1}{k_{eff}^{ri}}} \sum_{\substack{i=1 \\ i \neq n}}^{N} \frac{a_i W \mu_i}{k_{eff}^{ri}} \tag{11}$$

If the horizontal force sustained by the sliding plate is smaller than the frictional force at the n^{th} layer, $a_n W \mu_n$, the total stiffness of the rubber layers of the isolator, K_{eff}^{rb}, is a result of all layers of sole rubber materials connected in a series by excluding the contribution of this particular layer, which is not active. This is derived as:

$$\frac{1}{K_{eff}^{rb}} = \sum_{\substack{i=1 \\ i \neq n}}^{N} \frac{1}{k_{eff}^{ri}} = \frac{1}{k_{eff}^{r1}} + \frac{1}{k_{eff}^{r2}} + \frac{1}{k_{eff}^{r3}} + ... + \frac{1}{k_{eff}^{rn-1}} + \frac{1}{k_{eff}^{rn+1}} .. + \frac{1}{k_{eff}^{rN}} \tag{12}$$

Substitution of Eq. (12) into Eq. (11) leads to:

$$F = K_{eff}^{rb} u + K_{eff}^{rb} \sum_{\substack{i=1 \\ i \neq n}}^{N} \frac{a_i W \mu_i}{k_{eff}^{ri}} = K_{eff}^{rb} u + F_{eff}^{f} \tag{13}$$

where the equivalent frictional force of the entire system, F_{eff}^{f}, is given by:

$$F_{eff}^{f} = K_{eff}^{rb} \sum_{\substack{i=1 \\ i \neq n}}^{N} \frac{a_i W \mu_i}{k_{eff}^{ri}} \tag{14}$$

The relative displacement between the top and bottom of the i^{th} layer can be obtained by substituting Eq. (13) into Eq. (9) to arrive at:

$$u_i = \frac{F_i - a_i W \mu_i}{k_{eff}^{ri}} = \frac{F - a_i W \mu_i}{k_{eff}^{ri}} = \frac{1}{k_{eff}^{ri}} \left[\left(K_{eff}^{rb} u + K_{eff}^{rb} \sum_{\substack{i=1 \\ i \neq n}}^{N} \frac{a_i W \mu_i}{k_{eff}^{ri}} \right) - a_i W \mu_i \right] \tag{15}$$

Substitution of Eq. (15) into Eq. (4) leads to an enclosed area of the force-displacement loop of the sliding interfaces in the i^{th} layer such that:

$$A_{fi} = 4(\mu_i a_i W) u_i = \frac{4 \mu_i a_i W}{k_{eff}^{ri}} \left[\left(K_{eff}^{rb} u + K_{eff}^{rb} \sum_{\substack{i=1 \\ i \neq n}}^{N} \frac{a_i W \mu_i}{k_{eff}^{ri}} \right) - a_i W \mu_i \right] \tag{16}$$

The enclosed area of the force-displacement of the sole rubber of the i^{th} layer can be obtained with the aid of Eqs. (15) and (3) as:

$$A_{ri}=\frac{2\pi\xi_{ri}}{k_{eff}^{ri}}\left[\left(K_{eff}^{rb}u+K_{eff}^{rb}\sum_{\substack{i=1\\ i\neq n}}^{N}\frac{a_iW\mu_i}{k_{eff}^{ri}}\right)-a_iW\mu_i\right]^2 \tag{17}$$

Substituting Eqs. (16) and (17) into Eq. (7) results in the equivalent damping ratio of the entire isolator provided that the n^{th} layer is not active. This arrives at:

$$\xi_e=\frac{1}{2\pi K_{eff}u^2}\left\{\sum_{\substack{i=1\\ i\neq n}}^{N}\frac{2\pi\xi_{ri}}{k_{eff}^{ri}}\left[\left(K_{eff}^{rb}u+K_{eff}^{rb}\sum_{\substack{i=1\\ i\neq n}}^{N}\frac{a_iW\mu_i}{k_{eff}^{ri}}\right)-a_iW\mu_i\right]^2\right\}+\frac{1}{2\pi K_{eff}u^2}\left\{\sum_{\substack{i=1\\ i\neq n}}^{N}\frac{4\mu_ia_iW}{k_{eff}^{ri}}\left[\left(K_{eff}^{rb}u+K_{eff}^{rb}\sum_{\substack{i=1\\ i\neq n}}^{N}\frac{a_iW\mu_i}{k_{eff}^{ri}}\right)-a_iW\mu_i\right]\right\} \tag{18}$$

The vertical stiffness of the sole rubber in the i^{th} layer is given by the following [6].

$$k_{rV}^{i}=\frac{E_r^iA_{rubber}^i}{h_i} \tag{19}$$

where

$$E_r^i=6G_r^iS^2\lambda \tag{20}$$

Here, S is the shape factor of the i^{th} layer of rubber and equal to $\left(D_r^i-D_c^i\right)/4h_i$ for a circular cross section. In addition, λ is a parameter of the rubber layer to define the vertical stiffness of rubber as [6]:

$$\lambda=\frac{1}{(1-D_c^i/D_r^i)^2}\left[1+(D_c^i/D_r^i)^2+\frac{1-(D_c^i/D_r^i)^2}{\ln(D_c^i/D_r^i)}\right] \tag{21}$$

where D_r^i and D_c^i denote the diameters of the rubber layer and sliding core of the i^{th} layer of the isolator, respectively, as shown in Fig. 2.

The sliding plates in a single layer are connected in a series to result in the vertical stiffness of the i^{th} layer of the sliding core:

$$k_{fV}^{i}=\frac{k_{fV}^{f1}k_{fV}^{f2}k_{fV}^{f3}...k_{fV}^{fM-1}k_{fV}^{fM}}{k_{fV}^{f2}k_{fV}^{f3}...k_{fV}^{fM}+...+k_{fV}^{f1}k_{fV}^{f2}k_{fV}^{f3}..k_{fV}^{fM-1}} \tag{22}$$

where M is the total number of sliding plates in the i^{th} layer (a single layer with multiple sliding plates) and k_{fV}^{fj} denotes the vertical stiffness of the j^{th} sliding plate in the i^{th} layer of the sliding core.

The percentage of the total vertical load to be sustained by the sliding plates in a single layer can be obtained as:

$$a_i=\frac{k_{fV}^{i}}{k_{rV}^{i}+k_{fV}^{i}} \tag{23}$$

The total vertical stiffness of the i^{th} layer, k_V^i, is the sum of the vertical stiffness of rubber and sliding plates, given as:

$$k_V^i=k_{rV}^i+k_{fV}^i \tag{24}$$

The total vertical stiffness of the entire isolator is obtained by connecting all layers in a series as:

$$K_V=\frac{k_V^1k_V^2k_V^3....k_V^{N-1}k_V^N}{k_V^2k_V^3..k_V^N+...+k_V^1k_V^2k_V^3...k_V^{N-1}} \tag{25}$$

In the case of identical material properties including those of rubbers and sliding plates in all layers, we have $a=a_i$ and $\mu=\mu_i$ to yield the following [21]

$$\xi_e = \frac{\xi_e^{rb}}{1+\frac{aW\mu}{K_{eff}^{rb}u}} + \frac{2}{\pi}\frac{1}{1+\frac{K_{eff}^{rb}u}{aW\mu}} \tag{26}$$

The effective stiffness of the entire isolator, which combines rubber layers and the sliding core, is obtained by:

$$K_{eff} = K_{eff}^{rb} + \frac{aW\mu}{u} \tag{27}$$

As seen in (26), the equivalent damping ratio of the entire system approaches 63.7% whereas the displacement is approximately equal to zero. In addition, the equivalent damping ratio of the device approaches that of the sole rubber layers of the whole isolator if the displacement becomes extremely large. This is one of the advantages of this device, which provides a great value of damping ratio resulting from the sliding motion of sliding interfaces in the sliding core. The major parameters from Eq. (26) that affect the equivalent damping ratio of the entire isolation system are the following: the effective stiffness of all layers of rubber, sustained vertical loading of the sliding core, friction coefficients of sliding interfaces, equivalent damping ratio of rubber layers, and isolator displacement. The more the sustained vertical loading of the sliding core and friction coefficients of sliding interfaces are, the higher is the equivalent damping ratio. The low stiffness of sole rubber layers will increase the equivalent damping ratio of the isolator. The greater is the displacement, the smaller is the contribution from sliding motion and the larger is the contribution from rubbers to the equivalent damping ratio. The derived Eq. (26) reveals that softer rubber material, a higher friction coefficient, and greater vertical stiffness of the sliding core results in a higher damping ratio.

4 EXPERIMENTAL RESULTS

In this section, test results of scaled ARB specimens are presented to verify the concept proposed in this study. As Fig. 1 shows, the tested bearing was 140 mm in diameter and 85mm in height, and had a 3-mm cover, a sliding core of 45 mm in diameter, rubber of 5 mm in thickness in each layer, and a shim plate of 2 mm in thickness. Three sliding plates were included in each layer, including two each with 1.5-mm acetyl or polyoxymethylene (POM) and one steel plate of 2 mm in thickness, to total 5 mm that was identical to the thickness of the rubber layer. These sliding plates were positioned between two adjacent shim plates to produce two major sliding interfaces and were used to smooth the sliding motion of the sliding interfaces. In the specimen used in this study, the contact surface between the shim and sliding plates did not serve as a sliding interface to protect the adhesive and rubber material. Therefore, the sliding displacement of each sliding interface was a half of the rubber deformation in each layer.

Figures 5-8 show the hysteresis loops of the ARB specimen under a vertical load of 200 kN to lead to a vertical pressure of 13 MPa (130 kg/cm^2) on the tested bearing. Note that the shape factor of the bearing is as small as 4.75. Figs. 5-8 show horizontal displacements of 10, 20,30 and 40 mm, respectively, under a tested frequency of 0.7 Hz. These figures illustrate that the ARB seismic isolator possesses stable mechanical behaviour. In addition, as we predicted in the mathematical formulations, the frictional force contributed by the sliding core (note the force at zero displacement) can, provide remarkable damping to the isolator. Furthermore, the rubber material supplies stiffness and little damping to the device, which smoothes the corners of the hysteresis loops without dramatic changes in stiffness.

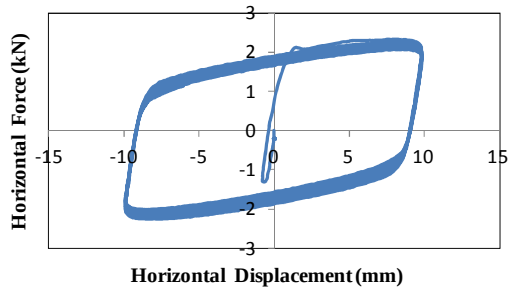

Figure 5 - Hysteresis loop of ARB under 10 mm displacement and 0.7 Hz frequency

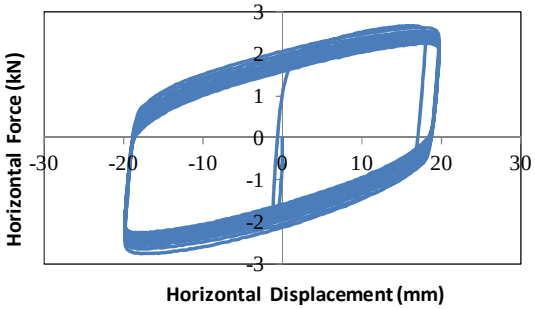

Figure 6 - Hysteresis loop of ARB under 20 mm displacement and 0.7 Hz frequency

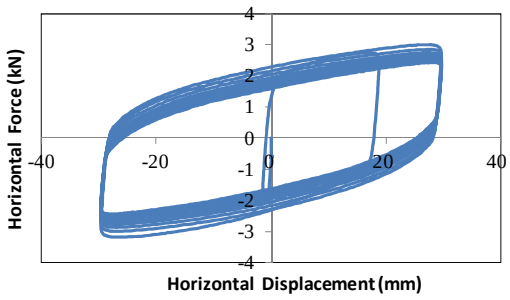

Figure 7 - Hysteresis loop of ARB under 30 mm displacement and 0.7 Hz frequency

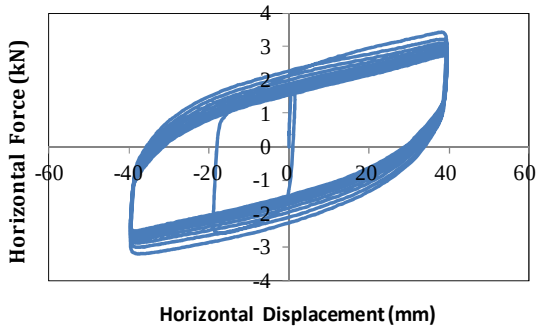

Figure 8 - Hysteresis loop of ARB under 40 mm displacement and 0.7 Hz frequency

Figure 9 shows an internal view of the ARB specimen after more than 200 cycle tests. This demonstrates that no damage occurred to the tested ARB specimen even after a large number of cycling loadings and a high testing velocity of 176 mm/sec. It also reveals that the proposed rubber bearing is durable.

Figure 9 - Internal view of an ARB specimen after more than 200 cycles of loadings

As Fig. 10 shows, the effective horizontal stiffness of the first cycle of the rubber bearing decreased with an increase in horizontal displacement. In addition, the testing velocity had insignificant effects on the effective horizontal stiffness of the first cycle. The equivalent damping ratio decreased from 54.5% at a displacement of 5 mm to 43.0% at a displacement of 40 mm, as shown in Fig. 11, whereas the horizontal displacement increased. However, the equivalent damping ratio of the ARB remained extremely high at a large displacement compared to that with the LRB

and high damping rubber bearing (HDRB). Figure 11 also reveals that the equivalent damping ratio of the first cycle is insensitive to the testing frequency. Figures 12 and 13 illustrate the changes in effective stiffness and equivalent damping ratio, respectively, under several cycling loadings and various testing frequencies. These figures illustrate that effective stiffness and the equivalent damping ratio decreased when loading cycles increased because the increased accumulated energy resulted in temperatures rising to weaken the material properties. Additionally, the higher the testing frequency (i.e., the testing velocity), the greater was the influence on material properties. Therefore, the functionality and design of a rubber bearing for engineering practice should consider the effects of temperature rising during an earthquake. However, the temperature effect on the proposed ARB isolator, which showed a less than 6.5% change in the first three cycles, is much less when compared to the LRB, which showed approximately a 25% difference in the first three cycles [22].

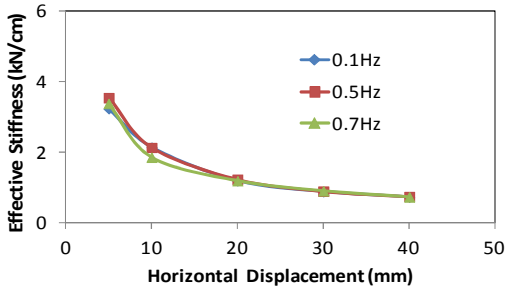

Figure 10 - Effective stiffness of the first cycle of ARB under various displacements and frequencies

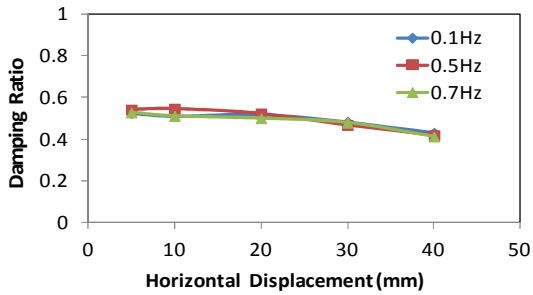

Figure 11 - Damping ratio of the first cycle of ARB under various displacements and frequencies

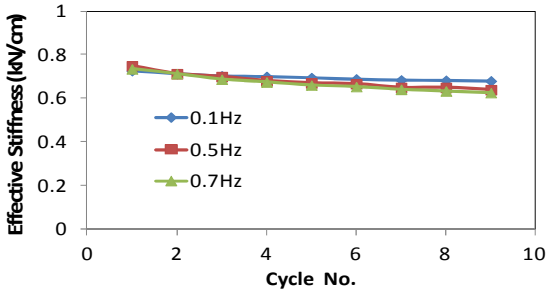

Figure 12 - Effective stiffness of ARB under 40 mm displacement and various frequencies

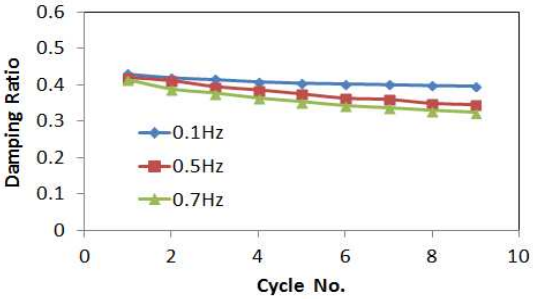

Figure 13 - Damping ratio of ARB under 40 mm displacement and various frequencies

5 CONCLUSION

An innovative seismic isolator known as the ARB was proposed in this study. The following conclusions can be drawn after theoretical and experimental investigations of the proposed device:

1. The ARB isolator adopts lead-free materials that are environment friendly.
2. The ARB isolator can sustain a high vertical pressure even with a small shape factor.
3. The ARB isolator possesses stable mechanical behavior and excellent durability.
4. The ARB isolator provides extremely high damping by means of a sliding mechanism in the sliding core.
5. The decrease in equivalent damping ratio of the proposed devices that occurs with an increased displacement is not considerable even during high velocity cyclical loadings.
6. Rising temperature during an earthquake can have a reduced effect on the ARB isolator

compared to that on the LRB.

7. The proposed rubber bearing is durable to sustain many reversal loadings.

In summary, theoretical derivations and experimental results reveal that the proposed ARB is a promising seismic isolator that can be used to solve problems encountered in LRBs and HDRBs.

REFERENCES

[1] Kelly, J. M. Aseismic base isolation: review and bibliography, *Soil Dynamics and Earthquake Engineering*, 1986; **5**(4): 202-216.

[2] Buckle, I. G. and Mayes, R. L. Seismic isolation: history, application, and performance —a world view, *Earthquake Spectra*, 1990; **6**(2): 161-201.

[3] Ibrahim, R. A. Recent advances in nonlinear passive vibration isolators, *Journal of Sound and Vibration*, 2008; **314**: 371-452.

[4] Tsai, C. S. *Advanced Base Isolation Systems for Light Weight Equipments*, Chapter 4, Earthquake-Resistant Structures- Design, Assessment and Rehabilitation, Edited by Abbas Moustafa, InTech, Croatia, 2012: 79-130.

[5] Tsai, C. S. Seismic isolation devices: history and recent developments, In *the 2015 ASME Pressure Vessels and Piping Conference, Seismic Engineering*, Tsai, C. S. (ed.), Boston, MA, U. S. A., 2015; Paper No. PVP2015-45068.

[6] Kelly, J. M. and Konstantinidis, D. A. *Mechanics of Rubber Bearings for Seismic and Vibration Isolation*, John Wiley & Sons, Ltd, , 2011.

[7] Tsai, C. S., Chiang, T. C., Chen, B. J. and Lin, B. S. An advanced analytical model for high damping rubber bearings, *Earthquake Engineering and Structural Dynamics*, 2003; **32**: 1373-1387.

[8] Robinson, W. H. *Cyclic Shear Energy Absorber*, US Patent No. 4117637, 1978.

[9] Zayas, V. A., Low, S. S. and Mahin, S. A. The FPS earthquake resisting system, Report, *EERC Technical Report*, 1987; UBC/EERC-87/01.

[10] Tsai, C. S. Finite element formulations for friction pendulum isolation bearings, *International Journal for Numerical Method in Engineering*, 1997; **40**: 29-49.

[11] Tsai, C. S, Chiang, T. C. and Chen, B. J. Finite element formulations and theoretical study for variable curvature friction pendulum system, *Engineering Structures*, 2003; **25**(14): 1719-1730.

[12] Tsai, C. S, Chiang, T. C. and Chen, B. J. Seismic behavior of MFPS isolated structure under near-fault sources and strong ground motions with long predominant periods, In the *2003 ASME Pressure Vessels and Piping Conference, Seismic Engineering*, Chen, J. C. (ed.), Cleveland, Ohio, U. S. A., 2003; **466**: 73-79.

[13] Tsai, C. S., Chiang, T. C. and Chen, B. J. Shaking table tests of a full scale steel structure isolated with MFPS, In *the 2003 ASME Pressure Vessels and Piping Conference, Seismic Engineering*, Chen, J. C. (ed.), Cleveland, Ohio, U. S. A., 2003; **466**: 41-47.

[14] Tsai, C. S., Chen, B. J., Pong, W. S. and Chiang, T. C. Interactive behavior of structures with multiple friction pendulum isolation system and unbounded foundations, *Advances in Structural Engineering, An International Journal*, 2004; **7**(6): 539-551.

[15] Tsai, C. S., Chiang, T. C. and Chen, B. J. Experimental evaluation piecewise exact solution for predicting seismic responses of spherical sliding type isolated structures, *Earthquake Engineering and Structural Dynamics*, 2005; **34**(9): 1027–1046.

[16] Tsai, C. S., Chen, W. S., Chiang, T. C. and Chen, B. J. Component and shaking table tests for full-scale multiple friction pendulum system, *Earthquake Engineering and Structural Dynamics*, 2006; **35**(11):1653–1675.

[17] Tsai, C. S., Lu, P. C., Chen, W. S., Chiang, T. C., Yang, C. T. and Lin, Y. C. Finite element formulation and shaking table tests of direction-optimized friction pendulum system, *Engineering Structures*, 2008; **30**(9): 2321-2329.

[18] Fenz, D. M. and Constantinou, M. C. Spherical sliding isolation bearings with adaptive behavior-theory, *Earthquake Engineering and Structural Dynamics*, 2008; **37**(2): 168-183.

[19] Morgan, T. A. and Mahin, S. A. The optimization of multi-stage friction pendulum isolators for loss mitigation considering a range of seismic hazard, In *the 14th World Conference on Earthquake Engineering*, Beijing, China, 2008; Paper No. 11-0070.

[20] Sterne L. *Improved Pneumatic Spring*, US Patent No. 87307, 1869.

[21] Tsai, C.S., Su, H.C. and Huang, W.C. An investigation of adaptive rubber bearings. In *the* 2016 *ASME Pressure Vessels and Piping Conference*, *Seismic Engineering*, Vancouver, British Columbia, Canada, 2016; Paper No. PVP2016-63087.

[22] Benzoni, G. and Casarotti, C. Performance of lead-rubber and sliding bearings under different axial load and velocity conditions, *Report No. SRMD–2006/05-rev3*, Charles Lee Powell Structural Research Laboratories CalTrans SRMD Test Facility, Department of Structural Engineering University of California, San Diego La Jolla, CA, USA, 2008.